



**HAL**  
open science

# Mineralogical differences in a temperate cultivated soil arising from different agronomic processes and plant K-uptake

Eleanor Bakker, Bruno Lanson, Nathaniel Findling, Michelle Wander, Fabien Hubert

► **To cite this version:**

Eleanor Bakker, Bruno Lanson, Nathaniel Findling, Michelle Wander, Fabien Hubert. Mineralogical differences in a temperate cultivated soil arising from different agronomic processes and plant K-uptake. *Geoderma*, 2019, 347, pp.210-219. 10.1016/j.geoderma.2019.04.010 . hal-02332083

**HAL Id: hal-02332083**

**<https://hal.science/hal-02332083>**

Submitted on 22 Oct 2021

**HAL** is a multi-disciplinary open access archive for the deposit and dissemination of scientific research documents, whether they are published or not. The documents may come from teaching and research institutions in France or abroad, or from public or private research centers.

L'archive ouverte pluridisciplinaire **HAL**, est destinée au dépôt et à la diffusion de documents scientifiques de niveau recherche, publiés ou non, émanant des établissements d'enseignement et de recherche français ou étrangers, des laboratoires publics ou privés.



Distributed under a Creative Commons Attribution - NonCommercial 4.0 International License

1 Mineralogical differences in a temperate cultivated soil arising from different  
2 agronomic processes and plant K-uptake

3

4 **Eleanor Bakker<sup>1,\*</sup>**

5 **Bruno Lanson<sup>1,\*</sup>**

6 **Nathaniel Findling<sup>1</sup>**

7 **Michelle M. Wander<sup>2</sup>**

8 **Fabien Hubert<sup>3</sup>**

9

10 (1) Univ. Grenoble Alpes, Univ. Savoie Mont Blanc, CNRS, IRD, IFSTTAR, ISTERre, F-38000  
11 Grenoble, France

12 (2) Dept Natural Resources and Environmental Sciences, Univ. Illinois at Urbana-  
13 Champaign, Urbana, Illinois, USA

14 (3) Univ. Poitiers, CNRS, IC2MP, F-86000 Poitiers, France

15

16 \* Corresponding author. E-mail: [bruno.lanson@univ-grenoble-alpes.fr](mailto:bruno.lanson@univ-grenoble-alpes.fr)

17

18 **Abstract**

19 Potassium (K) is an essential plant nutrient mainly present in the crystal structure of K-  
20 bearing soil minerals (K-feldspars, micas). To assess the evolution of (clay) mineralogy due to  
21  $K^+$  release from these minerals in continuously cultivated soils, samples were collected from  
22 long-term (1904-2014) field experiments submitted to contrasting crop rotations and  
23 amendments, with and without fertilisation. Soil samples were size-fractionated and  
24 mineralogy of the silt fraction and of clay subfractions was determined quantitatively by  
25 modelling X-ray diffraction (XRD) patterns. Clay subfractions were also analysed for their  
26 cation exchange capacity (CEC).

27 Mineralogical data indicate the stability of clay mineralogy and the increased abundance of  
28 the finest clay subfraction at the expense of coarser ones, regardless of agronomic practices  
29 or amount of K removed by plants. This increase is accompanied by an increase in the bulk  
30 clay CEC owing to the major contribution of the finest clay subfraction to this parameter.

31 Mineral dissolution, rather than alteration of mineral phases from coarse clay subfractions,  
32 most likely supplements K for plant nutrition in this soil. Dissolution is favoured over cation  
33 exchange owing to the dioctahedral character of micas and to their fine-grained  
34 granulometry. The observed long-term mineralogical resilience also indicates that part of  
35 plant nutrition is obtained from subsoil in a non K-limited context, whereas K supply through  
36 K-feldspar dissolution appears marginal.

37

38 **Keywords**

39 Potassium (K), plant nutrition, fertilisation, clay mineralogy, X-ray diffraction, long-term field  
40 experiment, Morrow Plots

41

42 **Highlights**

43 - Evolution of clay mineralogy was quantified in long-term experimental plots

44 - Different agronomical practices lead to contrasting K balances

45 - Clay mineralogy is stable over time in all subplots independent of K balance

46 - K is supplied by the dissolution of illite-rich coarse clay fractions and by subsoil

47 - Dioctahedral character of fined-grained micas favours dissolution over K-exchange

48

49 1. Introduction

50

51 Potassium (K) is an essential plant nutrient, playing roles in photosynthesis, water  
52 regulation and plant resistance to diseases (Marschner, 1995; Mengel et al., 2001). In soils,  
53 98-99 % of the potassium is found in the crystal structure of K-bearing minerals such as K-  
54 feldspars and micas (muscovite and biotite – Brouder, 2011; Mengel et al., 2001; Sparks,  
55 1987). In addition to climate, vegetation and factors like soil texture and pH, content and  
56 composition of soil solution, the nature and extent of weathering of K-bearing minerals  
57 present control the release of mineral K into solution through dissolution (Manning et al.,  
58 2017; Mengel et al., 2001; Sparks, 1987; Velde and Barré, 2009). Apart from this mineral  
59 pool, K is found also as an exchangeable cation (1-2 %) and in the soil solution (0.1-0.2 % –  
60 Brouder, 2011; Mengel et al., 2001; Sparks, 1987). Recent evaluations of K-testing methods  
61 and their interpretation suggest however that common categories used to describe K in soils  
62 (soluble, exchangeable, fixed) are not universally agreed upon or understood and that  
63 renewed exploration of mineralogical controls over K cycling and interlayer K contributions  
64 to plant nutrition are needed (Brouder, 2011).

65 Whilst exchangeable K, weakly held by the surface charges of clay minerals, and  
66 solution K are readily available for uptake by plants, release of mineral K which is present in  
67 the interlayer space of high-charge 2:1 clay minerals (micas) is thought to require depletion  
68 of exchangeable and solution K to low concentration (Smith and Scott, 1966). Concentrations  
69 associated with such K release from high-charge 2:1 clay interlayers are known to vary with  
70 the initial mica crystal structure, ranging from 2.3 to 16.8  $\mu\text{g mL}^{-1}$  for trioctahedral micas to  
71  $<0.1 \mu\text{g mL}^{-1}$  for dioctahedral muscovite and illite (Rausell-Colom et al., 1965; Sparks, 1987).  
72 The former K concentrations are compatible with those reported in soil solutions (4-40  $\mu\text{g}$

73 mL<sup>-1</sup>, Hinsinger, 1998) whereas the latter ones were only reported in the close vicinity  
74 (~1 mm) of plant roots where mineral dissolution may be significant (Jungk and Claassen,  
75 1997; Jungk et al., 1982). The possible release of mineral K<sup>+</sup> from mica interlayers and  
76 substitution by other cations is most often intimately related to clay mineralogical alteration,  
77 and more especially to the lowering of layer charge deficit (Hinsinger, 1998; Marschner,  
78 1995; Mortland et al., 1956; Tributh et al., 1987; Walker, 1950). Clay particle size may also  
79 influence the release of mineral K from clay minerals, which decreases with decreasing  
80 particle size (Doll et al., 1965; Reed and Scott, 1962; Scott and Reed, 1962b; Scott and Smith,  
81 1966).

82           The ability of plants to recover K from clay minerals has been observed in laboratory  
83 experiments from the vermiculitisation of K-bearing micas induced by plants grown on clay  
84 substrates (Barré et al., 2007, 2008a; Hinsinger and Jaillard, 1993; Hinsinger et al., 1992;  
85 Niebes et al., 1993). The extent to which plants can extract K varies notably with plant  
86 species, proximity to plant roots, soil solution chemistry and clay mineralogy (Barber and  
87 Mackay, 1986; Boyle and Voigt, 1973; Krafczyk et al., 1984; Marschner, 1995; Rengel and  
88 Damon, 2008; Schenk and Barber, 1980; Scott and Reed, 1962a). Long-term field  
89 experiments that began in the 19<sup>th</sup> and 20<sup>th</sup> centuries have led to the view that continuous  
90 cropping (30-135 years) increases smectite and/or vermiculite contents at the expense of  
91 mica/illite (Dissing Nielsen and Møberg, 1984; Møberg and Dissing Nielsen, 1983; Tributh et  
92 al., 1987). Surprisingly, Singh and Goulding (1997) observed an increase in the average K-  
93 concentration of soils from the Broadbalk continuous wheat plots established in 1843 at the  
94 Rothamsted Experimental Station (UK). The average total K-concentration increased from  
95 1.01 % (in 1856) to 1.10 % and 1.20 % in 1987 in non K-fertilised and K-fertilised plots,  
96 respectively, but no significant modification of clay mineralogy was detected.

97           In the aforementioned studies, clay mineralogy was determined using qualitative X-  
98 ray diffraction (XRD) methods that rely on the description of sharp and well-defined peaks  
99 associated with discrete clay minerals. Such qualitative description of XRD data does not  
100 recover comprehensive information about clay mineralogy and fails to measure  
101 contributions from mineral fractions potentially highly reactive: i) extremely small or crypto-  
102 crystalline and ii) complex interstratified minerals are essentially overlooked owing to their  
103 weakly modulated and faint diffraction signatures (Lanson, 2011). Over the last two decades,  
104 the peak decomposition method has improved and rationalised interpretation of XRD data,  
105 by decomposing profiles into elementary contributions that allow identifying contributions  
106 from both discrete and interstratified clay minerals (Lanson, 1997). Composition of the latter  
107 may be derived from the comparison with calculated patterns (e.g., Reynolds, 1985). As a  
108 result, shifts in the position of diffraction maxima and/or composition of mixed layers have  
109 been correlated to changes in K-concentration and to K-fertilisation (Barré et al., 2008a,  
110 2008b; Pernes-Debuyser et al., 2003; Velde and Peck, 2002). In their study of the Morrow  
111 Plots long-term experiment, Velde and Peck (2002) reported with this approach the  
112 apparent illite-depletion of the clay fraction from the continuous corn plot, whereas no  
113 evolution was detectable for the three year rotation (corn-oats-hay) plot. As calculated from  
114 yearly yields and fertiliser inputs, both plots exhibit similar K balance over the recent (1955-  
115 2005) period, however (Table 1 – Khan et al., 2014). On the other hand, these authors  
116 reported mineral stability in both the unfertilised crop rotation plot and the fertilised  
117 continuous corn plots despite negative and positive K balances, respectively (Table 1 – Khan  
118 et al., 2014). In any case, despite improving the description of clay mineral phases to include  
119 mixed layers and providing a proxy to their composition, the peak decomposition method  
120 does not account for the whole XRD profile and the obtained information remains essentially

121 qualitative. In addition, the decomposition method does not allow taking into account  
122 highly-disordered and/or interstratified contributions with small particle size.

123 More recently, a full-profile modelling method has been developed and used to  
124 characterise clay mineralogy of hydrothermal and diagenetic sequences (Aplin et al., 2006;  
125 Drits et al., 1997; Inoue et al., 2005; Lindgreen et al., 2000; McCarty et al., 2004; Sakharov et  
126 al., 1999a, 1999b). This approach has been adapted for soil samples and allows investigating  
127 soil mineralogy in a quantitative manner (Hubert et al., 2009, 2012; Viennet et al., 2015).  
128 Quantitative mineralogy appears especially important in the perspective of expected  
129 increases in fertilisation and competition for arable land resources, but also for the growing  
130 interest in CO<sub>2</sub> sequestration in cultivated soils (DeFries et al., 2010; Lambin and Meyfroidt,  
131 2011; Mueller et al., 2012). It is evident that comprehensive and quantitative descriptions of  
132 soil (clay) mineralogy are key to the assessment of soil responses to land-use changes or  
133 fertiliser inputs, given the contradictory results obtained from studies based on qualitative  
134 analyses of XRD data (see for example Dissing Nielsen and Møberg, 1984; Singh and  
135 Goulding, 1997; Tributh et al., 1987). The aim of the present study was thus to obtain a  
136 comprehensive compositional description of the clay minerals from the Morrow Plots by  
137 using full-profile XRD modelling and to compare and contrast, quantitatively, the effects of  
138 110 years of continuous plant-growth under different agronomic treatments on the nature  
139 and potassium content of clay minerals in the soil.

140

## 141 **2. Materials and Methods**

142

### 143 *2.1. Location and characteristics*



144

145           The Morrow Plots (MP) are located on the Urbana-Champaign campus of the  
146 University of Illinois (USA). The soil is an Aquic Argiudoll (loessic Flanagan silt loam – USDA  
147 soil taxonomy) developed on glacial till under temperate grassland vegetation. The MP  
148 receive an average of 968 mm precipitation (576 mm snowfall) per year, with a yearly  
149 average temperature of 11.1 °C (1904-2014 – MRCC, 2018). The MP have been under  
150 continuous cultivation since their establishment in 1876 and are accompanied by an  
151 extensive record of crop species, rotations, fertiliser inputs and yields (Aref and Wander,  
152 1998; Odell et al., 1984). Ten plots were established initially, and of these only three now  
153 remain. Each of the remaining plots is subject to a different crop rotation. Plot #3 is planted  
154 with corn (*Zea mays*) every year (C plots). Plot #4 (not included in this study) was initially  
155 planted in a two-yearly corn-oats (*Avena sativa*) rotation before being changed to a two-  
156 yearly corn-soybeans (*Glycine max*) rotation in 1967 to match regional cropping practices.  
157 Plot #5 is planted in corn-oats-hay on a three-yearly rotation (R plots), where the hay crop  
158 was red clover (*Trifolium pratense*) from 1904 to 1954 and alfalfa (*Medicago sativa*) from  
159 1955 onwards. Corn hybrids have been introduced in the rotations since 1937. Each of the  
160 plots is now divided into eight subplots, which each have a different fertilisation history. In  
161 the present study, samples were obtained from subplots which have remained unfertilised  
162 (CU and RU subplots) from the start of the experiment in 1876, and from subplots  
163 unfertilised between 1876 and 1954 which have received a nitrogen-phosphate-potassium  
164 (NPK) fertilisation treatment since 1955 (CF and RF subplots). Fertiliser is applied every year  
165 in CF subplot and once every three years (when corn is planted) in RF subplot. Fertilisation  
166 allowed for positive K balances in both CF and RF subplots, whereas Khan et al. (2014)  
167 computed negative balances for the equivalent unfertilised subplots (CU and RU subplots –

168 Table 1). Even for unfertilised subplots, soil K tests exhibit rather high values for soils  
169 cropped continuously for over a century (Table 1 – Aref and Wander, 1998). The seeding  
170 density of F subplots was also increased in 1955. Only minor adjustments have taken place  
171 since 1955, most notably a change from mouldboard to chisel plough in 1989 and an  
172 increase in seeding density in 2013. In 2013 and 2014, sampling took place from the 0-25 cm  
173 surface horizon on fallow plots just after harvest (late-September to October). Unfertilised  
174 samples from 1904 Plots #3 and #5, and both fertilised and unfertilised subplots from 1957,  
175 1980 and 1997 were collected from the soil archive at the U. of Illinois – Department of  
176 Agriculture (0-20 cm horizon). The latter samples were initially taken in the fall after harvest  
177 (Bob Dunker—Univ. of Illinois, personal communication). A complete description of the MP  
178 experimental fields can be found in Odell et al. (1984) and Aref and Wander (1998), where  
179 the samples in the current study are from NB (F) and NC (U) subplots of Plots #3 (C) and #5  
180 (R).

181

## 182 *2.2. Size-fractionation*

183

184 Air dried samples were first sieved at 2000  $\mu\text{m}$  to remove large organic fragments.  
185 Approximately 5 g, accurately weighed, of <2000  $\mu\text{m}$  soil material were dispersed via  
186 sonication in Milli-Q water (18.2  $\text{M}\Omega\text{ cm}^{-1}$ ) before being wet-sieved to 50  $\mu\text{m}$  (10 g of starting  
187 material were used for 2013 and 2014 samples). The 2000-50  $\mu\text{m}$  fraction obtained was  
188 dried at 50  $^{\circ}\text{C}$ . The <50  $\mu\text{m}$  fraction was centrifuged and flocculated with NaCl to reduce  
189 water content, then subjected to three overnight NaCl (2M) saturation cycles, followed by  
190 centrifugation and washing in dialysis tubes (Spectre/Por 6-8 kD membrane) until chloride  
191 free. Milli-Q water was systematically used for solution preparation, washing and dispersion

192 steps of sample fractionation and preparation. Sequential size fractionation was then  
193 performed by repeated centrifugation using a Beckmann-Coulter Avanti J-20XP centrifuge  
194 (procedure adapted from Hubert et al., 2012). A JS 4.3 swinging bucket rotor was used to  
195 separate 50-2 and <2  $\mu\text{m}$  fractions, with the 50-2  $\mu\text{m}$  fraction set aside to dry in the oven at  
196 50 °C. 10 repetitions were performed to obtain a clear supernatant, with dispersion via  
197 sonication (30 s) between successive cycles. 2-0.2, 0.2-0.05 and <0.05  $\mu\text{m}$  subfractions were  
198 obtained from repeated centrifugation of the initial <2  $\mu\text{m}$  fraction using a JS 24.38 swinging  
199 bucket rotor, with 10-15 cycles being necessary to obtain a clear supernatant for each  
200 subfraction. 1 M  $\text{CaCl}_2$  or KCl was then used to saturate subfractions with either  $\text{Ca}^{2+}$  or  $\text{K}^+$   
201 (three 24 h cycles) and samples were dialysed until chloride-free.

202

### 203 *2.3. Chemical analyses*

204

205 Bulk <2  $\mu\text{m}$  fractions from 1904, 1957 and 2014 (CF and RU subplots – CU and RU  
206 for 1904) were analysed for major and trace elements by inductively coupled plasma optical  
207 emission after sample preparation according to Carignan et al. (2001). These samples were  
208 analysed also for C, H, and N to determine their organic composition. Cation exchange  
209 capacity (CEC) analysis was also performed on these bulk <2  $\mu\text{m}$  fractions, and on 2-0.2, 0.2-  
210 0.05, and <0.05  $\mu\text{m}$  subfractions of 2014 samples (CF and RU subplots) using the cobalt  
211 hexamine method (Dohrmann and Kaufhold, 2009; Orsini and Remy, 1976).

212

### 213 *2.4. X-ray diffraction analysis*

214

215 X-ray diffraction (XRD) analysis of  $<2\ \mu\text{m}$  subfractions was performed on Ca-  
216 saturated oriented slides prepared via the pipette method, under air-dried (Ca-AD) or  
217 ethylene glycol (Ca-EG) saturated conditions. The mass of sample present on each slide was  
218 determined and used for subsequent XRD profile modelling. EG solvation was ensured  
219 through vapour exposure at  $50\ ^\circ\text{C}$  overnight. Oriented slides of selected K-saturated samples  
220 were also analysed following heat treatments at  $150$  or  $350\ ^\circ\text{C}$  for four hours (K-150 and K-  
221 350 samples, respectively). Samples were allowed to cool to room temperature before XRD  
222 data collection. XRD patterns of Ca-AD and Ca-EG samples were collected at 40 % relative  
223 humidity using a Bruker D8 equipped with an Anton Paar CHC+ chamber coupled to an MHG  
224 Messtechnik humidity controller. Patterns of K-150 and K-350 samples were collected at 5 %  
225 relative humidity with the same instrument. A Sol-XE Si (Li) solid state detector from Baltic  
226 Scientific Instruments was used to record intensities using  $\text{CuK}\alpha$  radiation over  $2$ - $50\ ^\circ 2\theta$   
227 using  $0.04\ ^\circ$  steps-and a counting time of 6 s per step for  $<2\ \mu\text{m}$  subfractions.  $50$ - $2\ \mu\text{m}$   
228 fractions were prepared for randomly oriented powder XRD analysis by milling with ethanol  
229 in a McCrone<sup>®</sup> micronising mill for 8 minutes. XRD data was collected over  $3$ - $90\ ^\circ 2\theta$  with  
230  $0.026\ ^\circ$  steps and a 8 s counting time per step using the Bruker D8 diffractometer. In all  
231 cases, the sizes of the divergence slit, the two Soller slits and the antiscatter slit were  $0.3\ ^\circ$ ,  
232  $2.5\ ^\circ$ ,  $2.5\ ^\circ$  and  $0.3\ ^\circ$ , respectively.

233

### 234 *2.5. XRD full-profile modelling*

235

236 Qualitative analysis of the  $<2\ \mu\text{m}$  subfractions was carried out as described in  
237 Bakker et al. (2018) where a detailed description of phase identification procedure is found.  
238 Full-profile XRD pattern modelling was then performed with the Sybilla programme

239 developed by Chevron™ (Aplin et al., 2006). Parameterisation and fitting procedure  
240 described in Bakker et al. (2018) were used for all samples and subplots from 1904-2014.  
241 Briefly, this modelling is based on the direct comparison between experimental and  
242 calculated 00ℓ XRD reflections, and fitting takes place via trial-and-error determination of  
243 structure factors to arrive at a single structure model which fits both the Ca-AD and Ca-EG  
244 XRD profiles of <2 µm subfractions (Drits et al., 1997; Hubert et al., 2009, 2012; Sakharov et  
245 al., 1999a, 1999b; Viennet et al., 2015). Such an approach relies on differences in layer-to-  
246 layer distances and structure factors for expandable layers arising from the different  
247 treatments (Ca-AD and Ca-EG) and leads to the determination of the proportion or weighted  
248 concentration of each independent phase in the sample.

249 Both discrete and interstratified contributions were considered. In the latter, factors  
250 such as layer types, their proportions and stacking sequences were refined. A single  
251 structure model which fits both the Ca-AD and Ca-EG XRD profiles of <2 µm subfractions is  
252 obtained at the end of the procedure. Discrete chlorite, kaolinite, illite and smectite were  
253 identified in <2 µm subfractions, in addition to up to seven mixed-layer contributions. The  
254 Profex interface for BGMN software (Doebelin and Kleeberg, 2015) was used for quantitative  
255 phase analysis through the Rietveld refinement of XRD patterns from the 50-2 µm fractions.

256

### 257 **3. Results**

258

#### 259 *3.1 Granulometry*

260

261 Results of size-fractionation are presented in Fig. 1. Recovery was 90.7-97.8 % of the  
262 starting weight (94.9 % on average). Individual results show a high and non-systematic

263 scatter between subplots for a given year, and for a single subplot in different years (Fig. S1).  
264 As a result of this variability, plots were assessed on the basis of the cropping practices;  
265 yearly averages were also considered. When averaged over all subplots for a given year, the  
266 2000-50  $\mu\text{m}$  fraction represents 7 % ( $\pm 2$  %), the 50-2  $\mu\text{m}$  fraction 64 % ( $\pm 2$  %), and the  
267  $<2$   $\mu\text{m}$  fraction 29 % ( $\pm 2$  %), for the years 1957 to 2014 (Fig. 1a). No systematic variation was  
268 observed between subplots for these fractions as a result of cropping practices (Figs. 1b-d,  
269 S1). These values are 4, 62, and 33 %, respectively, for 1904. The proportions of the 2-0.2,  
270 0.2-0.05 and  $<0.05$   $\mu\text{m}$  subfractions are also significantly different for 1904 compared to  
271 other years, most likely indicating sample grinding, consistent with the absence of soil  
272 aggregates in the sampled jar. When looking at the relative proportions of  $<2$   $\mu\text{m}$   
273 subfractions averaged over all subplots in a given year (Fig. 1d), there is a tendency for the  
274  $<0.05$   $\mu\text{m}$  subfraction to increase from  $\sim 9$  % of total sample mass in 1957 to  $\sim 13$  % in 2013-  
275 2014 (Fig. 1d). At the same time the relative mass of the 0.2-0.05  $\mu\text{m}$  subfraction decreases  
276 by  $\sim 2$  % whereas that of the 2-0.2  $\mu\text{m}$  subfractions is about stable (possible decrease by  $\sim 1$   
277 mass % – Figs. 1b-c). In addition, minor differences can be observed between the  
278 proportions of 2-0.2  $\mu\text{m}$  subfractions of C and R subplots, C subplots containing generally  
279 slightly less mass than corresponding R subplots (Fig. 1b). The inverse is observed for  
280  $<0.05$   $\mu\text{m}$  subfractions, where C subplots tend to have a greater proportion of  $<0.05$   $\mu\text{m}$   
281 subfraction than corresponding R subplots, except for recent years. These differences are  
282 statistically insignificant over the period studied, however.

283

### 284 3.2. Chemical analyses

285

286 Elemental analyses (Table 2) are consistent with a soil clay fraction dominated by  
287 phyllosilicates, with high levels of SiO<sub>2</sub> (43-46 %) and Al<sub>2</sub>O<sub>3</sub> (17-19 %). K levels were similar in  
288 both subplots in 1904 (2.13 % K<sub>2</sub>O), and did not vary between 1904 and 1957 (2.15 %). These  
289 levels are similar to those reported for clay fractions from a variety of soils of similar origin  
290 (Doll et al., 1965; Singh and Goulding, 1997). Whilst K decreased in clay fractions from both  
291 RU and CF subplots since 1957, the rate of decrease in RU subplots (-16 %) is faster than that  
292 in CF subplots (-7 %). In 1904, the C/N ratio of the RU subplot (11.3) was greater than that of  
293 CF (9.5). For both subplots, the C/N ratio has decreased since 1904 in line with the  
294 systematic loss of carbon. The carbon decrease rate has slowed in CF subplots since 1957  
295 and the introduction of fertilisation, whilst C levels continue to decrease at a similar rate  
296 post-1957 in RU subplots. The CEC of the <2 µm fraction measured for 1904 is similar for CU  
297 and RU subplots and remains constant between 1904 and 1957 (Table 2). From 1957, the  
298 CEC of both C and R subplots increases significantly (by ~15 %) from 48 to 55 cmol<sub>c</sub> kg<sup>-1</sup> in  
299 2014 for both CF and RU subplots. In addition, CEC of the <0.05 µm subfractions are akin in  
300 these two subplots at 81-82 cmol<sub>c</sub> kg<sup>-1</sup> (sample 2014) On the other hand, 0.2-0.05 and 2-  
301 0.2 µm subfractions demonstrate a difference of 7-8 cmol<sub>c</sub> kg<sup>-1</sup> favouring RU subplots (Table  
302 3).

303

### 304 *3.3. XRD qualitative analysis and XRD profile simulation*

305

306 Random powder XRD of 50-2 µm fractions and subsequent quantitative phase  
307 analysis found the mineralogy of the 50-2 µm fractions to be dominated by quartz (65-70 %)  
308 and potassium- (10-13 %) and plagioclase-feldspars (10-12 % – Fig. 2 and S2a-d, Table S1).  
309 Mica, kaolinite and chlorite also contribute in minor amounts to this fraction (~ 5, 1 and 2 %

310 respectively), whereas trace amounts (<1 %) of calcite, anatase and amphibole were also  
311 identified. There is no systematic variation in mineralogy of 50-2  $\mu\text{m}$  fractions from subplot-  
312 to-subplot or from year-to-year, with the exception of those of 1904 which had less mica and  
313 chlorite, presumably as the result of sample grinding (Table S1 and Figs. S2a-d). More  
314 especially, the relative abundances of K-bearing minerals (K-spars and micas) do not exhibit  
315 statistically significant evolutions with time and do not differ significantly as a function of  
316 agronomic practices (Table S1).

317 Full-profile modelling of the 2-0.2, 0.2-0.05 and <0.05  $\mu\text{m}$  subfractions for CF, CU,  
318 RF and RU subplots from 1904, 1957, 1980, 1997, 2013 and 2014 was performed using the  
319 structure model determined by Bakker et al. (2018) for the RU subplot. Similar contributions  
320 were used to model all <2  $\mu\text{m}$  subfractions from 1904-2014, with only limited modifications  
321 of their composition (layer-type proportions) and coherent scattering domain (CSD) sizes  
322 (Tables S2 and S3). The <0.05  $\mu\text{m}$  subfraction is dominated by randomly interstratified mixed  
323 layers in which illite, smectite and chlorite layers coexist (ISSCh). Two main contributions  
324 with contrasting illite contents (50 and 35 % in ISSCh 50 and ISSCh 35, respectively) coexist in  
325 this finest subfraction with two additional ISSCh contributions, one dominated by illite (ISSCh  
326 90), the other by smectite (ISSCh 5 – Tables S2c and S3c). Minor amounts of discrete  
327 smectite with extremely small CSD sizes and of kaolinite-illite (KI) complement the structure  
328 model of this <0.05  $\mu\text{m}$  subfraction. Except for discrete smectite, all contributions are  
329 present, with similar compositions and increased CSD sizes, in the 0.2-0.05 and 2-0.2  $\mu\text{m}$   
330 subfractions, together with discrete chlorite and discrete kaolinite. The peak at  $\sim 10 \text{ \AA}$  is  
331 accounted for by an additional illite-rich (ISSCh 80) mixed layer and discrete illite for the 0.2-  
332 0.05  $\mu\text{m}$  and the 2-0.2  $\mu\text{m}$  subfractions. Examples of the fit for 2014 CF and RU samples are  
333 shown in Fig. 3 whereas complete results of full-profile modelling of clay subfractions are



334 reported in Tables S2 and S3. Experimental XRD patterns recorded for the same subfraction  
335 from different subplots or years show little variation in either peak position or intensity (Figs.  
336 S3a-d, S4a-d, and S5a-d). Consistently, very little mineralogical difference was noted in the  
337 results of the full-profile modelling. Similarly, the composition of the different mixed layers  
338 varies only slightly between different subfractions. For example, for 2014 CF subplot ISSCh  
339 50 has a 52/26/22 layer composition in the <0.05  $\mu\text{m}$  subfraction which changes only slightly  
340 to 45/30/25 in the 2-0.2  $\mu\text{m}$  subfraction (Ca-EG treatment - Table S3). This is fairly  
341 representative of the compositional evolution determined between fine and coarse clay  
342 subfractions for all subplots and phases. The content of smectite layers tends to decrease for  
343 2-0.2  $\mu\text{m}$  subfractions compared to finer subfractions whilst the proportion of illite layers  
344 decreases with increasing size subfraction for ISSCh 50, 35 and 5 but increases in ISSCh 90  
345 and 80. These variations remain however marginal (~5 % of all layers at most). Similarly,  
346 composition of individual contributions appears stable as a function of time. For example,  
347 the composition of ISSCh 50 in the <0.05  $\mu\text{m}$  subfractions varies from 55/23/22 (1904 CU), to  
348 52/26/22 (1957 CF and 2014 CF), indicative of limited mineralogical evolution with time  
349 (Tables S2 and S3). Finally, K-spars are systematically present in the 2-0.2  $\mu\text{m}$  clay  
350 subfraction, with no apparent evidence for an evolution of their relative contribution with  
351 time and/or agronomic practices (Figs. S3a-d).

352           Within each subfraction, proportions of the different layer types can be computed  
353 from the summation over all contributions of the proportion of this specific layer type within  
354 a contribution multiplied by the relative proportion of this contribution in the subfraction  
355 (Fig. 4). Proportions of illite, smectite and chlorite layers all increase in <0.05  $\mu\text{m}$   
356 subfractions from 1957 to 2014, whilst the amount of kaolinite is stable (Fig. 4a). There is a  
357 concurrent decrease in the proportions of illite, smectite and chlorite layers with time in 0.2-

358 0.05  $\mu\text{m}$  subfractions, kaolinite content being again essentially stable (Fig. 4b). The  
359 proportion of illite layers in 2-0.2  $\mu\text{m}$  subfractions shows considerable scatter, making it  
360 difficult to define a clear trend. The proportion of illite layers is however stable or marginally  
361 decreasing with time, whilst smectite layers also show a marginal decrease and chlorite and  
362 kaolinite layers are stable. All evolutions observed remain too marginal given the time period  
363 studied (60 years) to be statistically significant, the uncertainty on mixed layer composition  
364 being about  $\pm 5\%$  of a given layer type (Hubert et al., 2012; Lanson et al., 2009). These  
365 evolutions appear to be mostly linked to the evolution of grain size distribution within the  
366  $< 2 \mu\text{m}$  fraction (Fig. 1). When all clay subfractions are considered jointly (Fig. 4d) the bulk  
367 clay mineralogy appears unchanged in the MP over the last 60 years of cropping, despite  
368 some intrinsic scatter.

369

## 370 **4. Discussion**

371

### 372 *4.1 Variability of results*

373

374 The granulometry results show significant variability between subplots for a given  
375 year, this variation being non-systematic on a year-to-year-basis (Figs. 1a and S1). This  
376 variability is most likely related to heterogeneity within the MP, despite their small size, and  
377 is further indicative of the absence of systematic impact of crop rotation or fertilisation.  
378 Sampling date scatter is possibly an additional source of variability that must be taken into  
379 consideration, as the exact timing of sampling post-harvest is not well-defined for historic  
380 samples (fallow period after harvest). Planting dates in the plots have varied by as much as  
381 147 days during the MP experiment, suggesting that harvest and therefore sampling dates

382 are also subject to considerable variation (Aref and Wander, 1998). Given that numerous  
383 studies have related changes in soil properties over periods as short as two weeks (Collignon  
384 et al., 2012; Haines and Cleveland, 1981; Marschner, 1995; Mengel et al., 2001; Peoples et  
385 al., 2014; Turpault et al., 2008; Weaver and Forcella, 1979), sampling date scatter may play a  
386 role in the observed granulometric and mineralogical variability. Furthermore, analysis of  
387 yield and climate data of the MP from 1888 to 1996 (Aref and Wander, 1998) revealed that  
388 yield was positively correlated not only with the temperature and precipitation of the  
389 preceding November and December but also with those of the preceding year. Climatic  
390 fluctuations also affect the distribution of plant roots in soils, and therefore the location of  
391 nutrient uptake, and this variation may be significant on a year-to-year basis (Marschner,  
392 1995; Mengel et al., 2001). The impacts of such climatic fluctuations on soil moisture and K  
393 availability may account, at least partially, for the difference observed between 2013 and  
394 2014 samples despite their small separation in time. Fertilisation treatments represent  
395 another source of variability. Whilst NPK fertilisation positively influenced average yields in F  
396 subplots, yield stability dropped when rates of fertiliser application were increased (Aref and  
397 Wander, 1998), reflecting variations in the short term availability of plant nutrients.

398

#### 399 *4.2. Evolution of (clay) mineralogy*

400

401 Following ~150 years of continuous cultivation, mineralogical differences in the MP  
402 are limited to a statistically insignificant increase of illite layers in 2-0.2  $\mu\text{m}$  subfractions from  
403 U subplots compared to F subplots and of smectite layers in  $<0.05 \mu\text{m}$  subfractions from C  
404 subplots compared to R ones (Fig. 4). In addition, K-spars are systematically present in the 2-  
405 0.2  $\mu\text{m}$  subfraction, with no evidence of dissolution with time even in U subplots which

406 exhibit strongly negative K-balances (Table 1; Figs. S3a-d), whereas the mineralogy of the  
407 coarser 50-2  $\mu\text{m}$  is essentially independent of time and agronomic practices (Table S1 and  
408 Figs. S2a-d). Despite the presence of K-spars in clay subfractions, which is favourable to their  
409 dissolution (Manning et al., 2017; Sadusky et al., 1987), their contribution to K supply is thus  
410 likely limited. This long-term mineralogical stability is consistent with previous reports  
411 demonstrating that mineralogical differences reported between rhizosphere and bulk soil  
412 after 40 days of corn cultivation did not persist longer than a growth cycle (130 days –  
413 Adamo et al., 2016). This long-term resilience most likely indicates that soil K reserves  
414 exceed the plough layer and that a significant proportion of plant nutrition is obtained from  
415 subsoil in a non K-limited context (Hinsinger et al., 2017; Kautz et al., 2013; Khan et al., 2014;  
416 Kuhlmann, 1990; Marschner, 1995). The absence of K-limitation is substantiated by the  
417 observed yield increase in U subplots following the introduction of hybrid crops in 1937 (Aref  
418 and Wander, 1998), increase allowed by the high K-levels measured in non-amended soils  
419 cropped continuously for decades (217 and 242  $\text{kg K ha}^{-1}$  measured in 1955 in R and C  
420 subplots, respectively – Table 1). Furthermore, these soil K-test values systematically  
421 increase with time whatever the K-balance in the considered plot (Table 1). In addition to  
422 the likely subsoil contribution, the similarity between F and U subplots may be favoured by  
423 the higher seeding density in the former – 20,000 and 30,000 plants  $\text{ha}^{-1}$  in CU and RU  
424 subplots, respectively, versus 40,000 and 60,000 plants  $\text{ha}^{-1}$  (for 1957-1977 and 1978-2013,  
425 respectively) in F subplots (Odell et al., 1984).

426           The lack of mineralogical evolution with time reported by Bakker et al. (2018) for RU  
427 subplots is upheld in the present study that considers different subplots and treatments,  
428 thus indicating a minimal influence of agronomic practices on soil mineralogy. These results  
429 are in agreement with Velde and Peck (2002) for R subplots, but the latter authors reported

430 a decrease in illite in the clay fraction of C subplots, based on XRD profile decomposition.  
431 The subtle variations in the position and shape of the 001 reflections in XRD profiles that  
432 were tentatively quantified by Velde and Peck (2002) were also observed in the present  
433 study. These were not systematic however and did not resolve into significant mineralogical  
434 differences following full-profile modelling, but rather contributed to the intrinsic sample  
435 variability.

436 Overall, the main evolution of clay mineralogy with time is the increased proportion  
437 of the  $<0.05\ \mu\text{m}$  subfraction from 1957 to 2014 for all subplots regardless of agronomic  
438 practices. This increase is accompanied by an increase of the bulk clay CEC owing to the  
439 major contribution of the finest subfraction to the CEC of the bulk  $<2\ \mu\text{m}$  fraction (Table 3).  
440 Contribution of soil organic matter to the CEC increase is likely minor despite decreasing C/N  
441 ratios with time. The minor character of this contribution is supported by similar CEC values  
442 measured for both CF and RU subplots despite the contrasting evolutions of their C/N ratios.  
443 The observed granulometric evolution of the bulk  $<2\ \mu\text{m}$  fraction is most likely due to  
444 mineral dissolution to supplement K for plant nutrition, as the K concentration decreases  
445 with time in this fraction for all subplots (Table 2). This decrease of K concentration is  
446 consistent with the negative K balances reported for U subplots over the period 1955-2005  
447 (Khan et al., 2014). These authors calculated positive K balances for F subplots, however,  
448 whereas a decrease in total K is also observed, a seemingly contradictory result. The mineral  
449 contributions to all subfractions being essentially similar in composition (Tables S2 and S3),  
450 the observed evolution in grain size likely takes place through dissolution of the phases  
451 present in the coarser 2-0.2 and 0.2-0.05  $\mu\text{m}$  subfractions rather than through their  
452 alteration or transformation. The breakdown of micro-aggregates initially present in these  
453 coarser subfractions could also account, at least partially, for the granulometric and CEC

454 evolutions observed with time. This effect is likely minor, however, owing to the systematic  
455 presence of minor amounts of carbonates in all soil samples despite the slightly acidic soil pH  
456 (Table S1). Furthermore, the steady decrease in C concentration from 1904-2014 is  
457 essentially disconnected from the CEC increase, that occurs mainly from 1957-2014 (Table  
458 2). Protection of  $<0.05\ \mu\text{m}$  particles by soil organic matter and sesquioxides, which are  
459 preferentially associated with this subfraction (e.g., Barré et al., 2014; Lützow et al., 2006;  
460 Singh et al., 2018), likely enhances the stability of this finest subfraction.

461

#### 462 *4.3. Mechanism of mineral K uptake by plants: Exchange Vs. dissolution*

463

464 As discussed above, both the absence of significant modification of clay mineralogy  
465 and the increased abundance of the finest clay subfraction ( $<0.05\ \mu\text{m}$ ) at the expense of the  
466 coarser ones ( $0.2-0.05$  and  $2-0.2\ \mu\text{m}$  subfractions) suggest that in the MP experiment K is  
467 most likely released from illite interlayer through dissolution rather than by exchange  
468 process. This inference raises the question of the prevalence of one process over the other  
469 and, more specifically, of the conditions leading to this predominance. Diffusion of K in illite  
470 interlayers at equilibrium in solutions similar to natural ones (de Haan et al., 1965; Nye,  
471 1972) implies a negligible contribution of interlayer K exchange. However, early studies have  
472 unambiguously shown that K can be removed from K-rich mica interlayers (muscovite, illite,  
473 phlogopite, biotite) through the sole exchange process (Reed and Scott, 1962; Scott, 1986;  
474 Scott and Reed, 1962a, 1962b; Scott and Smith, 1966; Smith and Scott, 1966). In this case,  
475 the driving force is the chemical gradient between mica interlayers and the solution, and the  
476 limiting factor is thus the K concentration in solution; threshold concentrations in solution

477 allowing K exchange range from 2.3 to 16.8  $\mu\text{g mL}^{-1}$  for trioctahedral micas to  $<0.1 \mu\text{g mL}^{-1}$   
478 for dioctahedral muscovite and illite (Rausell-Colom et al., 1965; Sparks, 1987). The higher  
479 content of structural Fe(II) in natural trioctahedral micas, compared to dioctahedral ones,  
480 may be responsible for these contrasting behaviours, as Fe(II) oxidation decreases layer  
481 charge deficit, thus favouring the exchange of interlayer  $\text{K}^+$  cations. Although low, these  
482 values allow for K exchange from trioctahedral micas in the laboratory (Hinsinger and  
483 Jaillard, 1993; Hinsinger et al., 1992; Niebes et al., 1993; Norouzi and Khademi, 2010), and in  
484 the field (Kapoor, 1972b; Wilson, 1966). The lower threshold concentrations determined for  
485 dioctahedral micas most likely hamper K exchange, however, consistent with the conclusions  
486 of Kapoor (1972a, 1972b), although root activity may induce such low concentrations in the  
487 rhizosphere (Hinsinger et al., 2011, 2017; Jungk and Claassen, 1997; Walker and Barber,  
488 1962). The concentrations of other nutrients (e.g., P and  $\text{NH}_4^+$ ) in solution may also have a  
489 key influence on the exchange of interlayer K, which can be totally inhibited in the presence  
490 of  $\sim 5 \mu\text{mol L}^{-1}$  of  $\text{NH}_4^+$ , a concentration common in natural soils (Springob, 1999).

491            Depending on the aforementioned experimental conditions, the kinetic competition  
492 between dissolution and exchange processes accounts of the heterogeneity of the results  
493 obtained from laboratory and field studies. Hinsinger and coworkers (Hinsinger et al., 1992,  
494 1993; Hinsinger and Jaillard, 1993) showed unambiguously the prevalence of exchange  
495 leading to the fast vermiculitisation of coarse trioctahedral mica (2-100  $\mu\text{m}$  phlogopite) by  
496 ryegrass and rape, possibly as the result of structural Fe(II) partial oxidation. Similar results  
497 were obtained by Naderizadeh et al. (2010) and Norouzi and Khademi (2010) also for  
498 trioctahedral micas (phlogopite and biotite) under alfalfa growth, whereas Vetterlein et al.  
499 (2013) reported a minor evolution of a reference illite (IMt-2, Clay Minerals Society  
500 Repository –  $<20 \mu\text{m}$  particles) to illite-expandable interstratification following 100 days of

501 alfalfa growth. Conversely, no mineralogical evolution was reported for a natural soil  
502 (Vetterlein et al., 2013) or muscovite (Naderizadeh et al., 2010; Norouzi and Khademi,  
503 2010), under similar experimental conditions. Muscovite dissolution even appears to be  
504 limited as alfalfa displays K deficiency symptoms (Norouzi and Khademi, 2010). Prevalence of  
505 dissolution was observed by Feigenbaum et al. (1975) using Ca and H-resins to release K  
506 from illite interlayers.

507           Kinetic competition between dissolution and exchange processes was investigated  
508 directly by Viennet et al. (2016) in the specific context of K-vermiculite aluminisation under  
509 acidic conditions (trioctahedral high-charge clay mineral, pH = 3). These authors concluded  
510 that despite the faster release of both exchangeable (at the particle surface) and non-  
511 exchangeable interlayer (i.e. mineral) K for the finest size fraction investigated (0.1-0.2  $\mu\text{m}$ ),  
512 the exchange process was rapidly stopped. Release of interlayer K subsequently proceeds  
513 through stoichiometric dissolution of this finest size fraction, whereas exchange remains  
514 active for coarser fractions (1-2  $\mu\text{m}$  and even more so for 10-20  $\mu\text{m}$ ). The decrease of K  
515 exchange when decreasing size fraction to clay size is consistent with experiments involving  
516 K release by chemical exchange (Doll et al., 1965; Reed and Scott, 1962; Scott and Reed,  
517 1962b; Scott and Smith, 1966) or by cropping (Doll et al., 1965), whereas the increased  
518 dissolution rate of finer subfractions is supported by experimental studies (Acker and  
519 Bricker, 1992; Bray et al., 2015). Results of the present study support a marginal release of  
520 interlayer K by exchange mechanisms and the prevalence of dissolution over exchange,  
521 consistent with this general discussion, as MP surface soils are typified by fine-grained  
522 dioctahedral micas and clay minerals (inset Fig. 2), both features being unfavourable to K  
523 exchange from mica interlayers.



524

## 525 **5. Conclusions**

526

527           Mineralogy of the silt fraction and of clay subfractions was determined  
528 quantitatively by modelling X-ray diffraction (XRD) patterns for a temporal series of top soil  
529 samples collected from the Morrow Plots long-term experimental fields. Samples from  
530 different subplots encompass a variety of cropping practices resulting in positive or negative  
531 K balances (fertilised and unfertilised subplots, respectively). Mineralogy of the different size  
532 fractions is essentially stable over time, independent of the overall K-balance and of  
533 agronomic practices, showing no significant decrease of the mica or K-spar relative  
534 abundances as the result of K uptake by plants. Within the clay fraction, the relative  
535 proportion of the finest (<0.05  $\mu\text{m}$ ) subfraction increases with time, together with the cation  
536 exchange capacity of the bulk <2  $\mu\text{m}$  fraction. This systematic granulometric evolution  
537 results from the dissolution of illite-rich coarse clay fractions. Prevalence of dissolution over  
538 K-exchange to supply plants with needed K most likely results from the dioctahedral  
539 character of fine-grained micas present in the Morrow Plots. Subsoil provide additional K for  
540 plant nutrition, whereas contribution of K-feldspars appears minimal in a non K-limited  
541 context. Finally, the improved description of (clay) mineralogy allowed by the full-profile  
542 modelling approach did not allow to evidence significant variation of (clay) mineralogy  
543 possibly resulting from cropping practices and related K-uptake.

544

## 545 **Acknowledgments**

546

547 Martine Lanson (ISTerre, Grenoble, France) has coordinated all chemical analyses and  
548 has performed CEC measurements. Chemical analyses were performed at the Service  
549 d'Analyse des Roches et des Minéraux (SARM-CNRS, Vandoeuvre-lès-Nancy, France) for  
550 major elements and at the Institut de Chimie des Substances Naturelles (ICSN – Gif sur Yvette,  
551 France) for C, H and N. Paolo Benavides (ISTerre, Grenoble, France) is thanked for size  
552 fractionation and XRD analysis of 1980 and 1997 samples. Tauhid B. Khan (ISTerre, Grenoble,  
553 France) is thanked for preliminary investigations of MP samples. Financial support from  
554 INSU/EC2CO program to FH and BL is acknowledged (Project Claie, 2015-2016). ISTerre is  
555 part of Labex OSUG@2020 (ANR10 LABX56).

556

## 557 **References**

558

- 559 Acker, J.G., Bricker, O.P., 1992. The influence of pH on biotite dissolution and alteration kinetics at  
560 low temperature. *Geochim. Cosmochim. Acta* 56, 3073-3092.
- 561 Adamo, P., Barré, P., Cozzolino, V., Di Meo, V., Velde, B., 2016. Short term clay mineral release and  
562 re-capture of potassium in a *Zea mays* field experiment. *Geoderma* 264, 54-60.
- 563 Aplin, A.C., Matenaar, I.F., McCarty, D.K., van Der Pluijm, B.A., 2006. Influence of mechanical  
564 compaction and clay mineral diagenesis on the microfabric and pore-scale properties of  
565 deep-water Gulf of Mexico Mudstones. *Clays & Clay Miner.* 54, 500-514.
- 566 Aref, S., Wander, M.M., 1998. Long-term trends of corn yield and soil organic matter in different crop  
567 sequences and soil fertility treatments on the Morrow Plots. *Adv. Agron.* 62, 153-198.
- 568 Bakker, E., Hubert, F., Wander, M.M., Lanson, B., 2018. Soil development under continuous  
569 agriculture at the Morrow Plots experimental fields from X-ray diffraction profile modelling.  
570 *Soil Syst.* 2, 46.
- 571 Barber, S.A., Mackay, A.D., 1986. Root growth and phosphorus and potassium uptake by two corn  
572 genotypes in the field. *Fert. Res.* 10, 217-230.

573 Barré, P., Fernandez-Ugalde, O., Virto, I., Velde, B., Chenu, C., 2014. Impact of phyllosilicate  
574 mineralogy on organic carbon stabilization in soils: incomplete knowledge and exciting  
575 prospects. *Geoderma* 235-236, 382-395.

576 Barré, P., Montagnier, C., Chenu, C., Abbadie, L., Velde, B., 2008a. Clay minerals as a soil potassium  
577 reservoir: observation and quantification through X-ray diffraction. *Plant Soil* 302, 213-220.

578 Barré, P., Velde, B., Catel, N., Abbadie, L., 2007. Soil-plant potassium transfer: impact of plant activity  
579 on clay minerals as seen from X-ray diffraction. *Plant Soil* 292, 137-146.

580 Barré, P., Velde, B., Fontaine, C., Catel, N., Abbadie, L., 2008b. Which 2 : 1 clay minerals are involved  
581 in the soil potassium reservoir? Insights from potassium addition or removal experiments on  
582 three temperate grassland soil clay assemblages. *Geoderma* 146, 216-223.

583 Boyle, J.R., Voigt, G.K., 1973. Biological weathering of silicate minerals. *Plant Soil* 38, 191-201.

584 Bray, A.W., Oelkers, E.H., Bonneville, S., Wolff-Boenisch, D., Potts, N.J., Fones, G., Benning, L.G., 2015.  
585 The effect of pH, grain size, and organic ligands on biotite weathering rates. *Geochim.*  
586 *Cosmochim. Acta* 164, 127-145.

587 Brouder, S., 2011. Potassium Cycling. In: J.L. Hatfield, T.J. Sauer (Eds.), *Soil Management: Building a*  
588 *Stable Base for Agriculture*. Soil Science Society of America, Madison, WI, pp. 79-102.

589 Carignan, J., Hild, P., Mevelle, G., Morel, J., Yeghicheyan, D., 2001. Routine Analyses of Trace  
590 Elements in Geological Samples using Flow Injection and Low Pressure On-Line Liquid  
591 Chromatography Coupled to ICP-MS: A Study of Geochemical Reference Materials BR, DR-N,  
592 UB-N, AN-G and GH. *Geostandards Newsletter* 25, 187-198.

593 Collignon, C., Ranger, J., Turpault, M.P., 2012. Seasonal dynamics of Al- and Fe-bearing secondary  
594 minerals in an acid forest soil: influence of Norway spruce roots (*Picea abies* (L.) Karst.). *Eur.*  
595 *J. Soil Sci.* 63, 592-602.

596 de Haan, F.A.M., Bolt, G.H., Pieters, B.G.M., 1965. Diffusion of Potassium-40 into an illite during  
597 prolonged shaking. *Soil Sci. Soc. Am. J.* 29, 528-530.

598 DeFries, R.S., Rudel, T., Uriarte, M., Hansen, M., 2010. Deforestation driven by urban population  
599 growth and agricultural trade in the twenty-first century. *Nature Geosci.* 3, 178.

600 Dissing Nielsen, J., Møberg, J.P., 1984. The influence of K-depletion on mineralogical changes in  
601 pedons from two field experiments and in soils from four pot experiments. *Acta Agric. Scand.*  
602 3, 391-399.

603 Doebelin, N., Kleeberg, R., 2015. Profex: a graphical user interface for the Rietveld refinement  
604 program BGMN. *J. Appl. Cryst.* 48, 1573-1580.

605 Dohrmann, R., Kaufhold, S., 2009. Three new, quick CEC methods for determining the amounts of  
606 exchangeable Calcium cations in calcareous clays. *Clays & Clay Miner.* 57, 338-352.

607 Doll, E.C., Mortland, M.M., Lawton, K., Ellis, B.G., 1965. Release of Potassium from Soil Fractions  
608 During Cropping. *Soil Sci. Soc. Am. J.* 29, 699-702.

609 Drits, V.A., Sakharov, B.A., Lindgreen, H., Salyn, A., 1997. Sequential structure transformation of illite-  
610 smectite-vermiculite during diagenesis of Upper Jurassic shales from the North Sea and  
611 Denmark. *Clay Miner.* 32, 351-371.

612 Feigenbaum, S., Shainberg, I., 1975. Dissolution of Illite—A possible mechanism of Potassium release.  
613 *Soil Sci. Soc. Am. J.* 39, 985-990.

614 Haines, S.G., Cleveland, G., 1981. Seasonal variation in properties of five forest soils in Southwest  
615 Georgia. *Soil Sci. Soc. Am. J.* 45, 139-143.

616 Hinsinger, P., 1998. How do plant roots acquire mineral nutrients? Chemical processes involved in  
617 the rhizosphere. *Adv. Agron.* 64, 225-265.

618 Hinsinger, P., Bell, M., White, P.J., 2017. Root traits and rhizosphere characteristics determining  
619 Potassium acquisition from soils. In: T.S. Murrell, R.L. Mikkelsen (Eds.), *Frontiers of Potassium*  
620 *Science Conference*. International Plant Nutrition Institute, Rome, Italy, pp. O289-O299.

621 Hinsinger, P., Brauman, A., Devau, N., Gérard, F., Jourdan, C., Laclau, J.-P., Le Cadre, E., Jaillard, B.,  
622 Plassard, C., 2011. Acquisition of phosphorus and other poorly mobile nutrients by roots.  
623 Where do plant nutrition models fail? *Plant Soil* 348, 29.

624 Hinsinger, P., Elsass, F., Jaillard, B., Robert, M., 1993. Root-induced irreversible transformation of a  
625 trioctahedral mica in the rhizosphere of rape. *J. Soil Sci.* 44, 535-545.

626 Hinsinger, P., Jaillard, B., 1993. Root-induced release of interlayer potassium and vermiculitization of  
627 phlogopite as related to potassium-depletion in the rhizosphere of ryegrass. *J. Soil Sci.* 44,  
628 525-534.

629 Hinsinger, P., Jaillard, B., Dufey, J.E., 1992. Rapid weathering of a trioctahedral mica by the roots of  
630 ryegrass. *Soil Sci. Soc. Am. J.* 56, 977-982.

631 Hubert, F., Caner, L., Ferrage, E., Meunier, A., 2012. Unraveling complex < 2  $\mu\text{m}$  clay mineralogy from  
632 soils using X-ray diffraction profile modeling on particle-size sub-fractions: Implications for  
633 soil pedogenesis and reactivity. *Amer. Mineral.* 97, 384-398.

634 Hubert, F., Caner, L., Meunier, A., Lanson, B., 2009. Advances in characterization of soil clay  
635 mineralogy using X-ray diffraction: from decomposition to profile fitting. *Eur. J. Soil Sci.* 60,  
636 1093-1105.

637 Inoue, A., Lanson, B., Marques Fernandes, M., Sakharov, B.A., Murakami, T., Meunier, A., Beaufort,  
638 D., 2005. Illite-smectite mixed-layer minerals in the hydrothermal alteration of volcanic  
639 rocks: I. One-dimensional XRD structure analysis and characterization of component layers.  
640 *Clays & Clay Miner.* 53, 423-439.

641 Jungk, A., Claassen, N., 1997. Ion Diffusion in the Soil–Root System. In: D.L. Sparks (Ed.), *Adv. Agron.*  
642 Academic Press, pp. 53-110.

643 Jungk, A., Claassen, N., Kuchenbuch, R., 1982. Potassium depletion of the soil-root interface in  
644 relation to soil parameters and root properties. In: A. Scaife (Ed.), *9<sup>th</sup> International Plant*  
645 *Nutrition Colloquium. Commonwealth Agricultural Bureaux, Warwick*, pp. 250-255.

646 Kapoor, B.S., 1972a. Weathering of micaceous minerals. *Norsk Geologisk Tidsskrift*, 52, 451-452.

647 Kapoor, B.S., 1972b. Weathering of micaceous minerals in some Norwegian podzols. *Clay Miner.* 9,  
648 383-394.

649 Kautz, T., Amelung, W., Ewert, F., Gaiser, T., Horn, R., Jahn, R., Javaux, M., Kemna, A., Kuzyakov, Y.,  
650 Munch, J.-C., Pätzold, S., Peth, S., Scherer, H.W., Schloter, M., Schneider, H., Vanderborght,  
651 J., Vetterlein, D., Walter, A., Wiesenberg, G.L.B., Köpke, U., 2013. Nutrient acquisition from  
652 arable subsoils in temperate climates: A review. *Soil Biol. Biochem.* 57, 1003-1022.

653 Khan, S.A., Mulvaney, R.L., Ellsworth, T.R., 2014. The potassium paradox: Implications for soil fertility,  
654 crop production and human health. *Renew Agric Food Syst* 29, 3-27.

655 Krafczyk, I., Trolldenier, G., Beringer, H., 1984. Soluble root exudates of maize: Influence of  
656 potassium supply and rhizosphere microorganisms. *Soil Biol. Biochem.* 16, 315-322.

657 Kuhlmann, H., 1990. Importance of the subsoil for the K nutrition of crops. *Plant Soil* 127, 129-136.

658 Lambin, E.F., Meyfroidt, P., 2011. Global land use change, economic globalization, and the looming  
659 land scarcity. *Proc. Nat. Acad. Sci.* 108, 3465-3472.

660 Lanson, B., 1997. Decomposition of experimental X-ray diffraction patterns (profile fitting): A  
661 convenient way to study clay minerals. *Clays & Clay Miner.* 45, 132-146.

662 Lanson, B., 2011. Modelling of X-ray diffraction profiles: Investigation of defective lamellar structure  
663 crystal chemistry. In: M.F. Brigatti, A. Mottana (Eds.), *Layered Mineral Structures and Their*  
664 *Application in Advanced Technologies. European Mineralogical Union Notes in Mineralogy.*  
665 *Mineralogical Society Great Britain & Ireland, London*, pp. 151-202.

666 Lanson, B., Sakharov, B.A., Claret, F., Drits, V.A., 2009. Diagenetic Smectite-to-Illite Transition in Clay-  
667 Rich Sediments: a Reappraisal of X-Ray Diffraction Results Using the Multi-Specimen Method.  
668 *Am. J. Sci.* 309, 476-516.

669 Lindgreen, H., Drits, V.A., Sakharov, B.A., Salyn, A.L., Wrang, P., Dainyak, L.G., 2000. Illite-smectite  
670 structural changes during metamorphism in black Cambrian Alum shales from the Baltic area.  
671 *Amer. Mineral.* 85, 1223-1238.

672 Lützow, M.v., Kögel-Knabner, I., Ekschmitt, K., Matzner, E., Guggenberger, G., Marschner, B., Flessa,  
673 H., 2006. Stabilization of organic matter in temperate soils: mechanisms and their relevance  
674 under different soil conditions – a review. *Eur. J. Soil Sci.* 57, 426-445.

675 Manning, D.A.C., Baptista, J., Sanchez Limon, M., Brandt, K., 2017. Testing the ability of plants to  
676 access potassium from framework silicate minerals. *Sci. Total Envir.* 574, 476-481.

677 Marschner, H., 1995. Mineral nutrition of higher plants. 2nd edition ed. Academic Press, London.

678 McCarty, D.K., Drits, V.A., Sakharov, B., Zviagina, B.B., Ruffell, A., Wach, G., 2004. Heterogeneous  
679 mixed-layer clays from the Cretaceous greensand, Isle of Wight, southern England. *Clays &  
680 Clay Miner.* 52, 552-575.

681 Mengel, K., Kirkby, E.A., Kosegarten, H., Appel, T. (Eds.), 2001. Principles of Plant Nutrition. Springer,  
682 Dordrecht, 849 pp.

683 Møberg, J.P., Dissing Nielsen, J., 1983. Mineralogical changes in soils used for Potassium-depletion  
684 experiments for some years in pots and in the field. *Acta Agric. Scand.* 33, 21-27.

685 Mortland, M.M., Lawton, K., Uehara, G., 1956. Alateraton of Biotite to Vermiculite by plant growth.  
686 *Soil Sci.* 82, 477-482.

687 MRCC, 2018. Cli-MATE: Midwestern Regional Climate Centre Application Tools Environment.

688 Mueller, N.D., Gerber, J.S., Johnston, M., Ray, D.K., Ramankutty, N., Foley, J.A., 2012. Closing yield  
689 gaps through nutrient and water management. *Nature* 490, 254.

690 Naderizadeh, Z., Khademi, H., Arocena, J.M., 2010. Organic matter induced mineralogical changes in  
691 clay-sized phlogopite and muscovite in alfalfa rhizosphere. *Geoderma* 159, 296-303.

692 Niebes, J.-F., Dufey, J., Jaillard, B., Hinsinger, P., 1993. Release of nonexchangeable potassium from  
693 different size fractions of two highly K-fertilized soils in the rhizosphere of rape (*Brassica  
694 napus* cv Drakkar). *Plant Soil* 155-156, 403-406.

695 Norouzi, S., Khademi, H., 2010. Ability of alfalfa (*Medicago sativa* L.) to take up potassium from  
696 different micaceous minerals and consequent vermiculitization. *Plant Soil* 328, 83-93.

697 Nye, P.H., 1972. The measurement and mechanism of ion diffusion in soils. VIII — A theory for the  
698 propagation of changes of pH in soils. *J. Soil Sci.* 23, 82-92.

699 Odell, R.T., Melsted, S.W., Walker, W.M., 1984. Changes in organic Carbon and Nitrogen of Morrow  
700 plots soils under different treatments, 1904–1973. *Soil Sci.* 137, 160-171.

701 Orsini, L., Remy, J., 1976. Utilisation du chlorure de cobaltihexamine pour la détermination  
702 simultanée de la capacité d'échange et des bases échangeables des sols. *Bull. AFES - Sci Sol* 4,  
703 269-275.

704 Peoples, M.B., Richardson, A.E., Simpson, R.J., Fillery, I.R.P., 2014. Soil: Nutrient Cycling. In: N.K. Van  
705 Alfen (Ed.), *Encyclopedia of Agriculture and Food Systems*. Academic Press, Oxford, pp. 197-  
706 210.

707 Pernes-Debuyser, A., Pernes, M., Velde, B., Tessier, D., 2003. Soil mineralogy evolution in the INRA 42  
708 Plots experiment (Versailles, France). *Clays & Clay Miner.* 51, 577-584.

709 Rausell-Colom, J.A., Sweatman, T.R., Wells, C.B., Norrish, K., 1965. Studies in the artificial weathering  
710 of mica. In: E.G. Hallsworth, D.V. Crawford (Eds.), *Experimental Pedology*. Univ. Nottingham  
711 11<sup>th</sup> Easter School Agricultural Science. Butterworths, London, pp. 40-72.

712 Reed, M.G., Scott, A.D., 1962. Kinetics of potassium release from biotite and muscovite in sodium  
713 tetraphenylboron solutions. *Soil Sci. Soc. Am. J.* 26, 437-440.

714 Rengel, Z., Damon, P.M., 2008. Crops and genotypes differ in efficiency of potassium uptake and use.  
715 *Physiol. Plantarum* 133, 624-636.

716 Reynolds, R.C., Jr, 1985. NEWMOD: A computer program for the calculation of one-dimensional  
717 patterns of mixed-layered clays. Reynolds, R.C., Jr, Hanover, NH.

718 Sadusky, M.C., Sparks, D.L., Noll, M.R., Hendricks, G.J., 1987. Kinetics and Mechanisms of Potassium  
719 Release from Sandy Middle Atlantic Coastal Plain Soils<sup>1</sup>. *Soil Sci. Soc. Am. J.* 51, 1460-1465.

720 Sakharov, B.A., Lindgreen, H., Salyn, A., Drits, V.A., 1999a. Determination of illite-smectite structures  
721 using multispecimen X-ray diffraction profile fitting. *Clays & Clay Miner.* 47, 555-566.

722 Sakharov, B.A., Lindgreen, H., Salyn, A.L., Drits, V.A., 1999b. Mixed-layer kaolinite-illite-vermiculite in  
723 North Sea shales. *Clay Miner.* 34, 333-344.

724 Schenk, M.K., Barber, S.A., 1980. Potassium and phosphorus uptake by corn genotypes grown in the  
725 field as influenced by root characteristics. *Plant Soil* 54, 65-76.

726 Scott, A.D., 1986. Mechanisms of potassium release by soil minerals, XIII. Congress of International  
727 Society of Soil Science, Hamburg, Germany, pp. 1144-1154.

728 Scott, A.D., Reed, M.G., 1962a. Chemical extraction of Potassium from soils and micaceous minerals  
729 with solutions containing Sodium Tetraphenylboron: II. Biotite. *Soil Sci. Soc. Am. J.* 26, 41-45.

730 Scott, A.D., Reed, M.G., 1962b. Chemical extraction of Potassium from soils and micaceous minerals  
731 with solutions containing Sodium Tetraphenylboron: III. Illite. *Soil Sci. Soc. Am. J.* 26, 45-48.

732 Scott, A.D., Smith, S.J., 1966. Susceptibility of interlayer Potassium in micas to exchange with Sodium.  
733 *Clays & Clay Miner.* 14, 69-81.

734 Singh, B., Goulding, K.W.T., 1997. Changes with time in the potassium content and phyllosilicates in  
735 the soil of the Broadbalk continuous wheat experiment at Rothamsted. *Eur. J. Soil Sci.* 48,  
736 651-659.

737 Singh, M., Sarkar, B., Sarkar, S., Churchman, J., Bolan, N., Mandal, S., Menon, M., Purakayastha, T.J.,  
738 Beerling, D.J., 2018. Stabilization of soil organic Carbon as influenced by clay mineralogy. In:  
739 D.L. Sparks (Ed.), *Adv. Agron.* Academic Press, pp. 33-84.

740 Smith, S.J., Scott, A.D., 1966. Extractable Potassium in grundite illite: I. Method of extraction. *Soil Sci.*  
741 102, 115-122.

742 Sparks, D.L., 1987. Potassium dynamics in soils. In: B.A. Stewart (Ed.), *Advances in soil science.*  
743 Springer Verlag, New York, pp. 1-63.

744 Springob, G., 1999. Blocking the release of potassium from clay interlayers by small concentrations of  
745  $\text{NH}_4^+$  and  $\text{Cs}^+$ . *Eur. J. Soil Sci.* 50, 665-674.

746 Tributh, H., Boguslawski, E.V., Lieres, A.V., Steffens, D., Mengel, K., 1987. Effect of Potassium removal  
747 by crops on transformation of illitic clay minerals. *Soil Sci.* 143, 404-409.

748 Turpault, M.P., Righi, D., Uterano, C., 2008. Clay minerals: Precise markers of the spatial and  
749 temporal variability of the biogeochemical soil environment. *Geoderma* 147, 108-115.

750 Velde, B., Barré, P., 2009. *Soils, plants and clay minerals*. Springer, Berlin, Heidelberg.

751 Velde, B., Peck, T., 2002. Clay mineral changes in the Morrow experimental plots, University of  
752 Illinois. *Clays & Clay Miner.* 50, 364-370.

753 Vetterlein, D., Kühn, T., Kaiser, K., Jahn, R., 2013. Illite transformation and potassium release upon  
754 changes in composition of the rhizosphere soil solution. *Plant Soil* 371, 267-279.

755 Viennet, J.-C., Hubert, F., Ferrage, E., Tertre, E., Legout, A., Turpault, M.-P., 2015. Investigation of clay  
756 mineralogy in a temperate acidic soil of a forest using X-ray diffraction profile modeling:  
757 Beyond the HIS and HIV description. *Geoderma* 241-242, 75-86.

758 Viennet, J.-C., Hubert, F., Tertre, E., Ferrage, E., Robin, V., Dzene, L., Cochet, C., Turpault, M.-P., 2016.  
759 Effect of particle size on the experimental dissolution and auto-aluminization processes of K-  
760 vermiculite. *Geochim. Cosmochim. Acta* 180, 164-176.

761 Walker, G.F., 1950. Trioctahedral minerals in the soil-clays of North-East Scotland. *Mineral. Mag.* 29,  
762 72-84.

763 Walker, J.M., Barber, S.A., 1962. Absorption of potassium and rubidium from the soil by corn roots.  
764 *Plant Soil* 17, 243-259.

765 Weaver, T., Forcella, F., 1979. Seasonal variation in soil nutrients under six Rocky Mountain  
766 vegetation types. *Soil Sci. Soc. Am. J.* 43, 589-593.

767 Wilson, M.J., 1966. The weathering of biotite in some Aberdeenshire soils. *Mineral. Mag.* 36, 1080-  
768 1093.

769



770 **Figure Captions**

771

772 **Fig. 1.** Grain size distributions obtained for 1904-2014 soil samples with the sequential  
773 fractionation procedure described in the text; a) Size distribution of the <2 mm fraction  
774 averaged over all subplots for a given year and normalised to 100 %, b-d) Abundances of clay  
775 subfractions for different agronomic practices. Solid black lines represent the yearly average  
776 for each subfraction (b: 2-0.2  $\mu\text{m}$ , c: 0.2-0.05  $\mu\text{m}$ , and d: <0.05  $\mu\text{m}$  subfraction); esd's on illite  
777 content are calculated from all subplots for a given year. Colour figure is available online.

778

779 **Fig. 2.** Selection of quantitative phase analysis performed with the Rietveld method on XRD  
780 patterns of sample 2014 (CF and RU subplots). Experimental data is represented by grey  
781 crosses, and solid black lines indicate the calculated intensity. Difference plots are solid grey  
782 lines underneath. Inset b) shows the position of the 06,33 reflection for the bulk <2  $\mu\text{m}$   
783 fraction of sample 2014 (RU subplot). Colour figure is available online.

784

785 **Fig. 3.** Selection of XRD full-profile modelling of clay subfractions. a) 2014 RU (left) and b)  
786 2014 CF (right) subplots. Ca-EG and Ca-AD are shown at the top and the bottom of the  
787 Figure, respectively. XRD patterns of 2-0.2, 0.2-0.05 and <0.05  $\mu\text{m}$  subfractions are shown  
788 from top to bottom for each treatment. Symbols as in Fig. 2. Quartz, feldspar, and *hk*  
789 contributions from phyllosilicates are indicated by solid black, open black and solid grey  
790 triangles respectively. These contributions were not taken into account during the modelling  
791 procedure. The vertical grey bars represents an increase in intensity of the high-angle region  
792 compared to the 2–22° 2 $\theta$  angular range ( $\times 2$  scale factor). Colour figure is available online.

793

794 **Fig. 4.** Relative abundances of illite, smectite, chlorite and kaolinite layers in the different  
795 clay subfractions (a: <0.05  $\mu\text{m}$ , b: 0.2-0.05  $\mu\text{m}$ , and c: 2-0.2  $\mu\text{m}$ , c: 0.2-0.05  $\mu\text{m}$ ) and in the  
796 bulk <2  $\mu\text{m}$  fraction (d). Yearly averages are represented by lines, symbols representing  
797 different agronomic practices for illite. Smectite is represented in grey to enhance the  
798 difference between illite and smectite. Note the y-axis scale in d) is twice that of the other

799 plots. Colour figure is available in Bakker\_Clay\_Miner\_MP\_Geoderma\_ESM.pdf Online  
800 Resource (Fig. ESM6); esd's on illite content are calculated for C, R, U, and F subplots for a  
801 given year.

802

803

**Table 1**

804

Impact of agronomical practices on K content and balance.

	CU	CF	RU	RF
Exchangeable K content in surface soil (0-15 cm) from 1955 (kg K ha <sup>-1</sup> ) <sup>a</sup>	242		217	
Soil K content (1969-1995) <sup>b</sup> kg K ha <sup>-1</sup>	250.7	317.2	241.7	266.5
Exchangeable K content in surface soil (0-15 cm) from 2005 (kg K ha <sup>-1</sup> ) <sup>a</sup>	403	354	382	332
K balance (1955-2005) <sup>c</sup> kg K ha <sup>-1</sup>	-892	+539	-1088	+249

<sup>a</sup> Exchangeable K contents determined in 1955 and 2005 samples (0-15 cm – Aref and Wander, 1998)

<sup>b</sup> K contents are average values from samples collected annually from 1969-1995 (0-15 cm – Aref and Wander, 1998)

<sup>c</sup> K balance values are computed from yearly yields and fertiliser inputs. See (Khan et al., 2014) for details.

805

**Table 2**

806

Results of CEC and elemental analyses for the bulk Na-saturated <2  $\mu\text{m}$  fraction from samples 1904, 1957 and 2014.

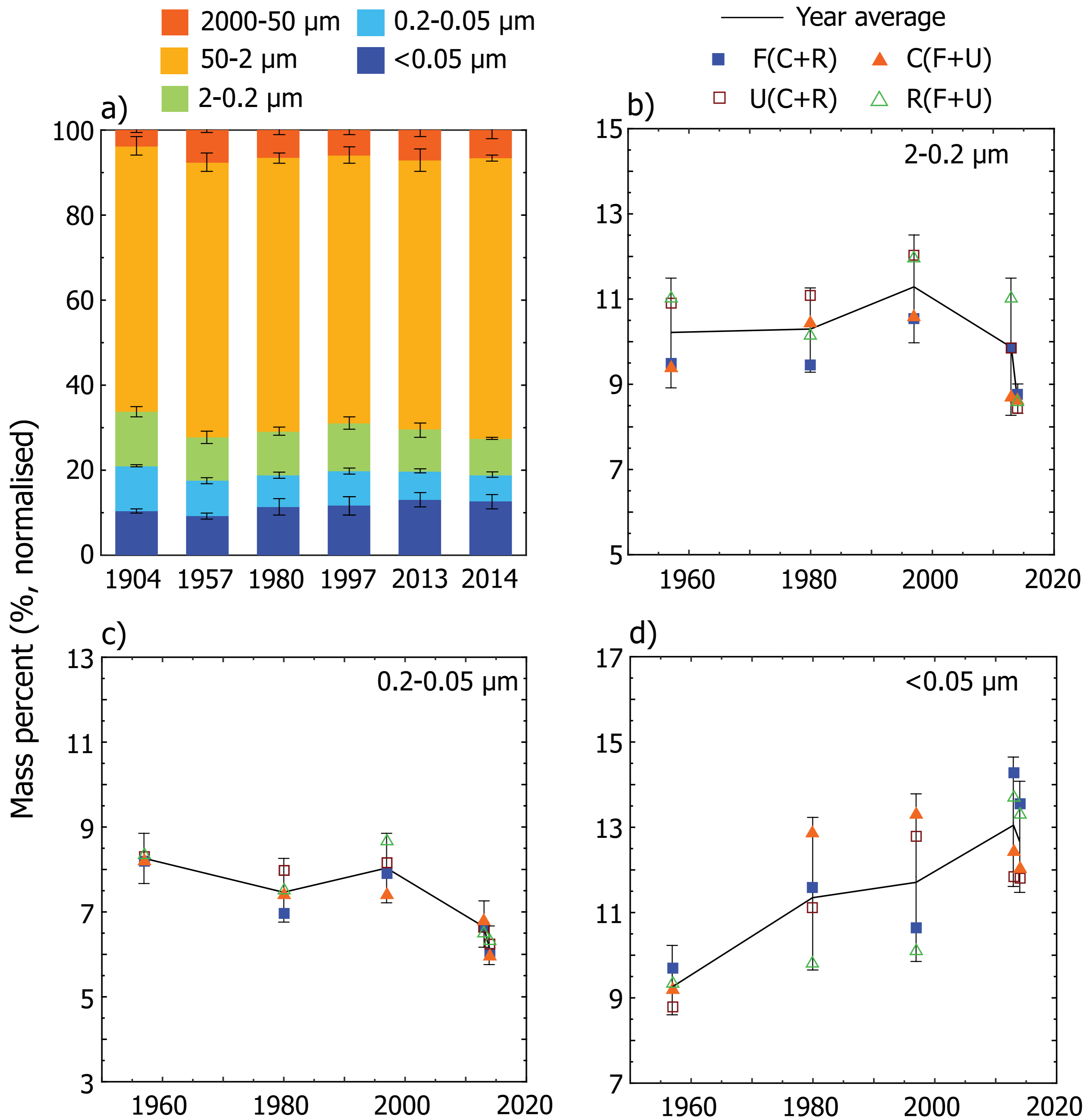
Year	Fraction	CEC cmol <sub>c</sub> kg <sup>-1</sup>	C %	N %	C/N	K <sub>2</sub> O %	Na <sub>2</sub> O %	MgO %	CaO <sup>1</sup> %	TiO <sub>2</sub> %	Fe <sub>2</sub> O <sub>3</sub> %	MnO %	P <sub>2</sub> O <sub>5</sub> %	SiO <sub>2</sub> %	Al <sub>2</sub> O <sub>3</sub> %	LOI %
1904 RU	<2 $\mu\text{m}$	45.5	6.47	0.58	11.25	2.15	0.25	1.78	0.08	0.79	8.56	0.07	0.28	45.57	17.25	21.63
1904 CF	<2 $\mu\text{m}$	47.8	6.29	0.66	9.53	2.11	0.21	1.82	0.07	0.91	8.71	0.13	0.26	44.64	17.40	22.34
1957 RU	<2 $\mu\text{m}$	47.9	6.18	0.57	10.93	2.18	0.22	1.78	0.07	0.82	8.33	0.08	0.29	46.56	17.30	20.20
1957 CF	<2 $\mu\text{m}$	47.9	6.18	0.49	9.09	2.13	0.17	1.97	0.06	0.84	9.12	0.13	0.24	45.96	18.75	22.38
2014 RU	<2 $\mu\text{m}$	55.2	5.79	0.60	9.65	1.83	0.15	1.91	-	0.65	8.85	0.06	0.32	43.09	18.10	19.12
2014 CF	<2 $\mu\text{m}$	55.3	4.24	0.49	8.73	1.98	0.17	2.01	-	0.75	9.20	0.06	0.43	45.38	19.06	22.70

Note: The low value of Ca is due to Na-saturation of samples prior to analysis.

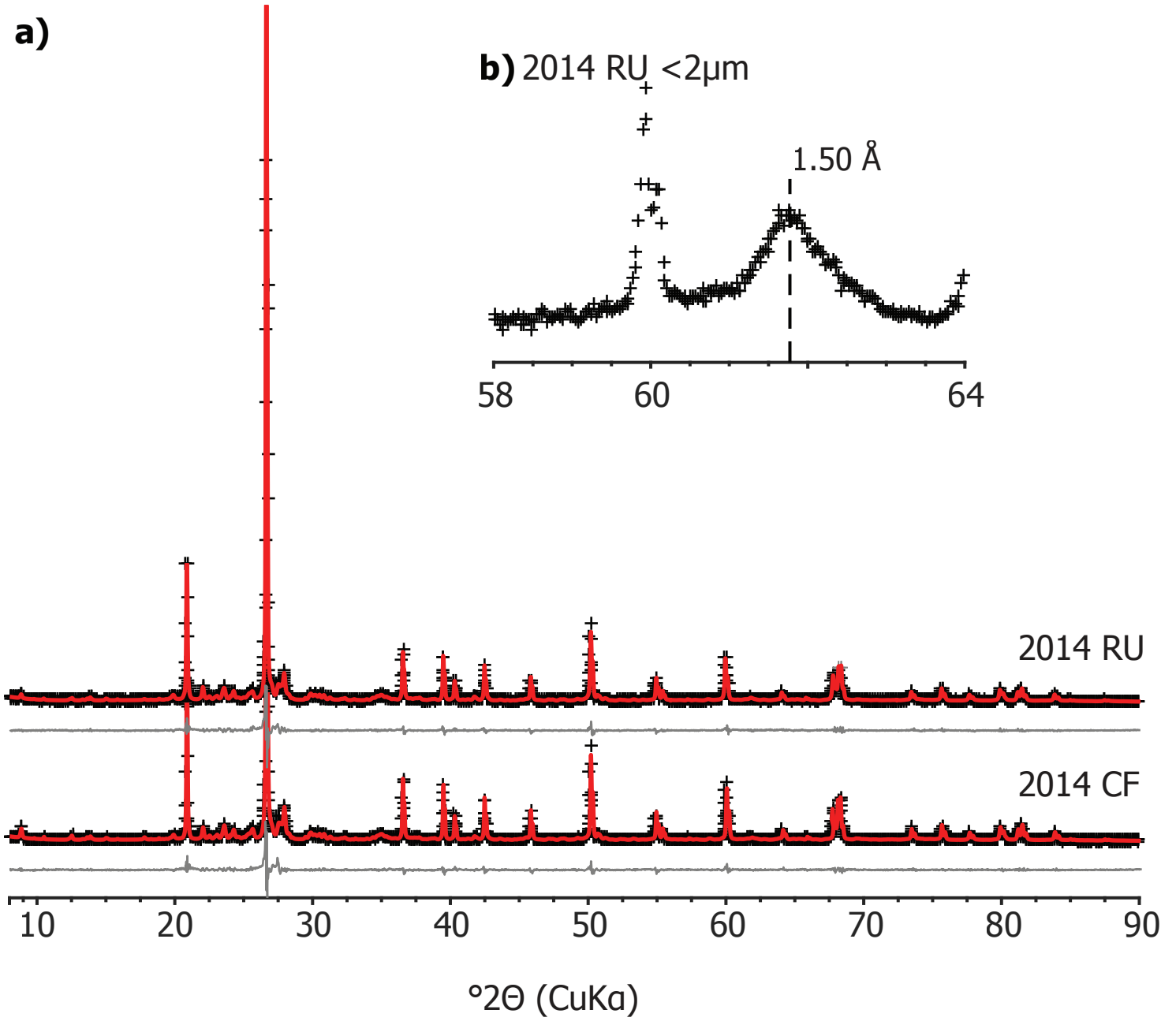
807 **Table 3**  
 808 Measured and calculated CEC values for sample 2014 clay-size fractions and  
 809 subfractions. The calculated CEC value for the bulk <2  $\mu\text{m}$  fraction is a weighted  
 810 average of the CEC values measured for the different subfractions.

Subfraction	2014 RU			2014 CF		
	CEC (meas.) $\text{cmol}_c \text{kg}^{-1}$	Rel. prop. (wt %)	CEC (calc.) $\text{cmol}_c \text{kg}^{-1}$	CEC (meas.) $\text{cmol}_c \text{kg}^{-1}$	Rel. prop. (wt %)	CEC (calc.) $\text{cmol}_c \text{kg}^{-1}$
<2 $\mu\text{m}$	55.2	-	57.8	55.3	-	52.9
2-0.2 $\mu\text{m}$	22.1	30.7	-	14.0	31.8	-
0.2-0.05 $\mu\text{m}$	58.6	25.6	-	51.3	23.0	-
<0.05 $\mu\text{m}$	82.2	43.8	-	81.2	45.1	-

811



a)



a) 2014 CF

+++ Experimental data — Best fit — Difference

b) 2014 RU

